Heavy Flavor Measurements at STAR

Róbert Vértesi for the STAR Collaboration

Nuclear Physics Institute ASCR, 25068 Řež, Czech Republic

Abstract

We present a selection of recent heavy flavor results from the STAR experiment. Measurements of D^0 and D^* meson production in $\sqrt{s}$=200 and 500 GeV p+p, as well as in $\sqrt{s_{NN}}$=200 GeV d+Au, Au+Au and 193 GeV U+U collisions are presented and implications on the production mechanism are discussed. We report on the production and elliptic flow of electrons from semi-leptonic decays of heavy flavor hadrons in $\sqrt{s_{NN}}$=39, 62.4 and 200 GeV Au+Au collisions. Nuclear modification of J/ψ production in $\sqrt{s_{NN}}$=39, 62.4 and 200 GeV Au+Au, and 193 GeV U+U, and of Υ in 200 GeV d+Au, Au+Au, and 193 GeV U+U collisions are compared to theoretical models. Finally we discuss the prospects of heavy flavor measurements with the recent detector upgrades.

1. Introduction

In ultrarelativistic heavy ion collisions, a phase transition occurs from hadronic matter into a state of deconfined quarks and gluons [1, 2]. Properties of this latter state of matter, dubbed as the strongly interacting Quark Gluon Plasma (sQGP), have been a subject of extensive measurements at the Relativistic Heavy Ion Collider (RHIC) in the past decade and a half. The RHIC Beam Energy Scan (BES) program Phase I. was dedicated to the search of turn-off signatures of the sQGP [3]. On the other hand, significantly improved luminosity of RHIC in the recent years, paired with continuous detector development allows one to turn to rare probes, such as heavy flavor production, which are complementary to observables of light hadrons and provide us with a deeper understanding of the strong interaction.

1.1. Heavy flavor at RHIC energies

Charm and bottom quarks are produced in hard QCD processes early in the interaction, and, due to their large masses, their number is virtually unaffected in the later stages of the reaction. Heavy flavor quarks therefore provide a unique means of exploring the properties of

the sQGP. Open heavy flavor yields at different momenta are sensitive to the energy loss mechanism of partons. Azimuthal anisotropy measurements may supply us with additional information about the degree of thermalization of the medium.

Quarkonium states are expected to be subject to sequential melting due to the screening of the $q\bar{q}$ potential in the sQGP, and provide access to thermodynamical properties of the medium [4]. Production of charmonia is abundant and therefore it is relatively easy to measure them with precision. However, several effects concurrent to sequential melting, such as feed-down, recombination in the sQGP and co-mover absorption in the hadronic phase, influence measured yields [5]. The interplay between these effects can be understood by comprehensive measurements at different energies and in different colliding systems. Bottomonium measurements are of special interest because, contrary to charm quarks, the effect of bottom pair recombination and co-mover absorption is negligible at RHIC energies [6].

1.2. Experiment

The STAR detector at RHIC is a compound experiment of several subsystems that provides a full az-

imuthal coverage at mid-rapidity ($|\eta|$<1). In the analyses discussed below, momentum measurement of charged particles, as well as particle identification based on energy loss via ionization, is done using the Time Projection Chamber (TPC). Charged particle identification is aided by the Time of Flight detector (TOF) at low p_T. The Barrel Electromagnetic Calorimeter (BEMC) is used for energy measurement and further identification of electrons. The Vertex Position Detector (VPD) provides trigger for the minimum bias (MB) data. A detailed description of STAR is in Ref. [7]. Results of Refs. [8–14] are summarized here along with some recent preliminary results.

2. Open heavy flavor measurements

Currently, STAR measures open heavy flavor through two different channels. One is the direct reconstruction of charmed mesons from their hadronic decays ($D^0 \rightarrow K^- \pi^+$ or $D^{*+} \rightarrow D^0 \pi^+ \rightarrow K^- \pi^- \pi^+$ and their charge conjugated counterparts) [8, 9]. D^0 and D^* meson production was measured in $\sqrt{s}$=200 and 500 GeV p+p, as well as D^0 in $\sqrt{s_{NN}}$=200 GeV Au+Au and $\sqrt{s_{NN}}$=193 GeV U+U MB collisions. The invariant yields are determined in the following way: the invariant mass peak is reconstructed from the decay products, the combinatorial background is subtracted using event mixing (D^0) or swapped-sign background (D^*), and the residual background is removed with a sideband fit. The raw spectrum is then corrected for acceptance and efficiency. This method provides direct access to the kinematics of the charmed meson. However, such events are difficult to trigger on, and without secondary vertex detection capabilities, the combinatorial background level is high.

The other way is to measure *non-photonic electrons* (NPE) from semileptonic decays of charm and bottom [10], eg. $D^0 \rightarrow e^+ \nu_e K^-$. Such processes typically have branching ratios two times larger than hadronic channels, and high-p_T electrons are easily triggered on in the BEMC using a *high tower* (HT) trigger. It is, however, not possible to directly separate charm and bottom contribution without secondary vertex reconstruction. The main background for this process is the so-called photonic electrons (PE), $e^- e^+$ pairs from decays of light hadrons and from photon conversion in detector material. The PE contribution is determined from data.

2.1. D^0 and D^* production

Precision p+p measurements are essential as a benchmark for theoretical calculations as well as a baseline for nuclear modification. Uncertainty in extrapolation
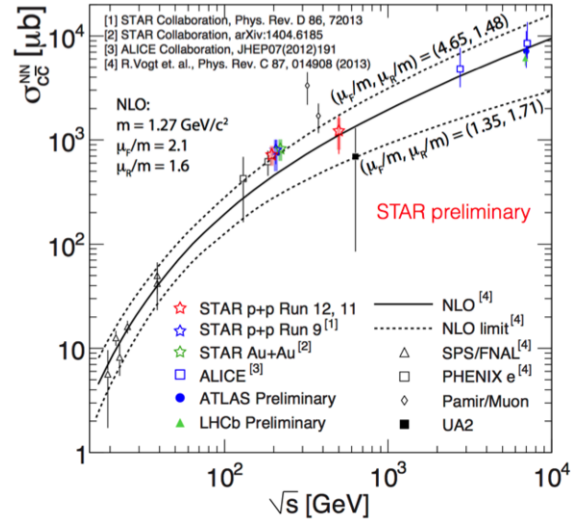

Figure 1: Charm production cross sections in p+p collisions versus collision energy $\sqrt{s}$, compared to world data and pQCD calculations [16].

of the D^0 and D^* spectra towards lower momenta used to be one of the main sources of the systematic uncertainty on the total production cross section [8]. Recent high-statistics measurements at $\sqrt{s}$=200 GeV constrained the shape of the spectrum by extending the range with a new 0<p_T<0.7 GeV/c point. Fig. 1 shows previously published charm production cross sections $d\sigma_{c\bar{c}}^{NN}$ at $\sqrt{s_{NN}}$=200 GeV, as well as new 200 and 500 GeV data. STAR data points follow the trend of world data and are described by pQCD FONLL calculations [16].

Fig. 2 shows a comparison of $d\sigma_{c\bar{c}}^{NN}$ in $\sqrt{s_{NN}}$=200 GeV p+p, d+Au and Au+Au collisions. The total cross section follows scaling with the number of binary collisions (N_{bin}), supporting the picture that charm is produced early, in perturbative processes. Accordingly, nuclear modification factor R_{AA} of the D^0 mesons, in Fig. 3 (a), exhibit no significant modification in peripheral collisions at $\sqrt{s_{NN}}$=200 GeV [9]. In more central collisions, however, a different structure emerges: while higher-p_T D^0 R_{AA} shows similar suppression to that of light mesons [17, 18], a characteristic hump-shaped enhancement appears in the 1<p_T<2 GeV/c range. The 10% most central data are compared to several models in Fig. 3 (c). High-p_T suppression of the charmed mesons indicates a strong charm–medium interaction [27]. The low-momentum enhancement can be understood by models that include charm–light quark coalescence [20–22] and allow for charm to pick up radial flow. A model prediction without charm–light quark coalescence [23] differs significantly from obser-
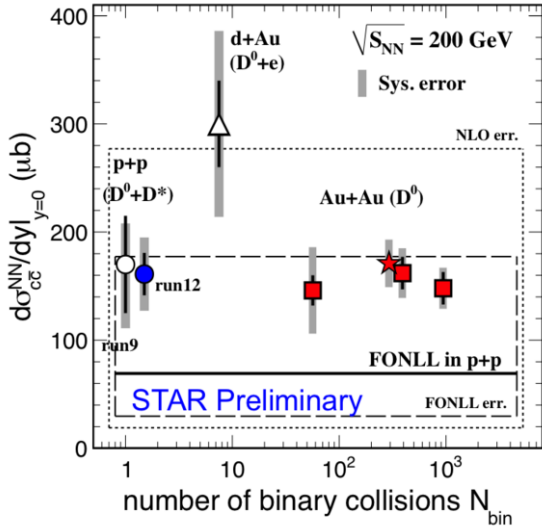
Figure 2: The STAR results at $\sqrt{s}$=200 and 500 GeV are compared to different experiments and an NLO model. *Right:* Charm production cross section in STAR p+p, d+Au and Au+Au collisions versus the number of binary collisions N_{bin}.
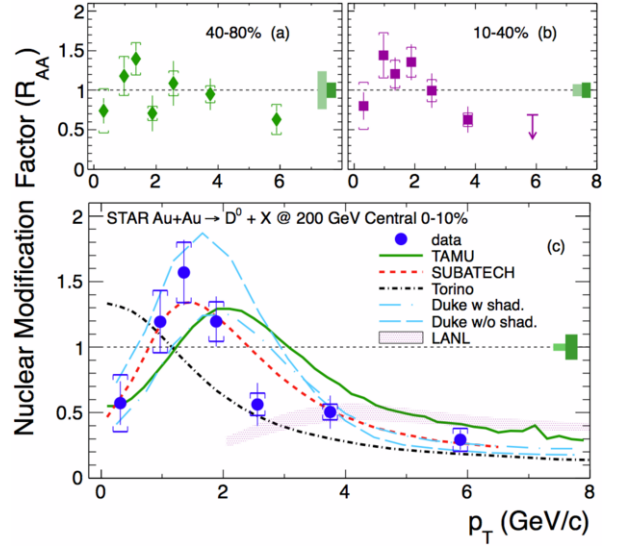

Figure 3: Nuclear modification factor of D^0 in Au+Au collisions versus p_T in (a) peripheral, (b) mid-central and (c) central collisions [9], the latter compared to several popular models [20–23, 27].

vations in the low-momentum range [9]. Model calculations of Ref. [22] hint that *cold nuclear matter* (CNM) effects play an important role.

Uranium ions are heavier than gold and have a prolate shape, and therefore they extend the STAR measurements up to higher number of participant nucleons N_{part}. It is estimated [15] that, on average, an approximately 20% higher Bjorken energy density is achieved in central U+U than in central Au+Au collisions. The R_{AA} of D^0 mesons with $p_T>3$ GeV/c in top-energy Au+Au and U+U versus N_{part} is shown in Fig. 4. The trend of increasing suppression with N_{part}, observed in Au+Au collisions, is continued in the U+U data. This trend is completely consistent with high-p_T light mesons [17].

2.2. Non-photonic electrons at different energies

Fig. 5 shows a significant suppression of non-photonic electron yield in central $\sqrt{s_{NN}}$=200 GeV Au+Au collisions, that is similar to light mesons. The results are compared to several energy loss mechanism models [24–28]. Although gluon radiation scenario [24] is quite successful in describing energy loss of light hadrons, it appears not to be enough alone to explain the observed high-p_T NPE suppression. The azimuthal anisotropy parameter v_2 (also called elliptic flow) is found to be non-zero, and significantly above the non-flow estimation at low momenta [10]. It is to be noted that those models that are in better agreement with the NPE R_{AA} come short in describing v_2 at the same time.

The picture emerging from recent lower energy measurements is, however, radically different from top RHIC energy. Fig. 6 shows the R_{AA} of NPE in $\sqrt{s_{NN}}$=62.4 GeV Au+Au collisions. The p+p reference used here is from pQCD calculations with k_T-factorization technique [29], which gives an upper limit for NPE production in p+p collisions [30]. The R_{AA} is generally flat, showing no NPE suppression in $\sqrt{s_{NN}}$=62.4 GeV Au+Au collisions. Fig. 7 shows the NPE elliptic flow in $\sqrt{s_{NN}}$ =39, 62.4 and 200 GeV Au+Au collisions. While at top RHIC energy one observes substantial flow, v_2 is consistent with zero in the case of the two lower energies, and differs significantly from top energy results in the 0.5<p_T<1 GeV/c range. These results suggest that the effect of the thermalized, hot matter does not dominate heavy flavor production anymore at 62.4 GeV and below.

3. Quarkonium results

Quarkonia are reconstructed via the dielectron decay channel (J/ψ→e$^-$e$^+$, Υ→e$^-$e$^+$). Minimum bias data were used in the BES J/ψ analyses [11], with an event mixing background subtraction. At $\sqrt{s_{NN}}$=200 GeV, both MB and HT triggered data were used to maximize luminosity at high-p_T [12]. HT triggered data were used in the Υ analyses [14]. Like-sign pair combinatorial background subtraction was applied. There is a substantial background contribution from Drell-Yan and open
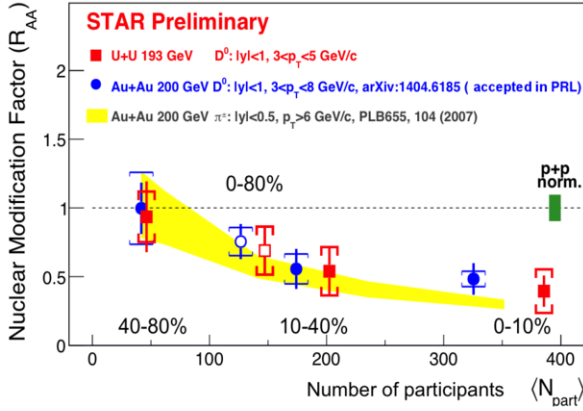
Figure 4: Nuclear modification factor of $p_T > 3$ GeV/c D^0 mesons in Au+Au (dots) and in preliminary U+U measurements (squares) for minimum bias collisions (open symbols) as well as at different N_{part} values (solid symbols).
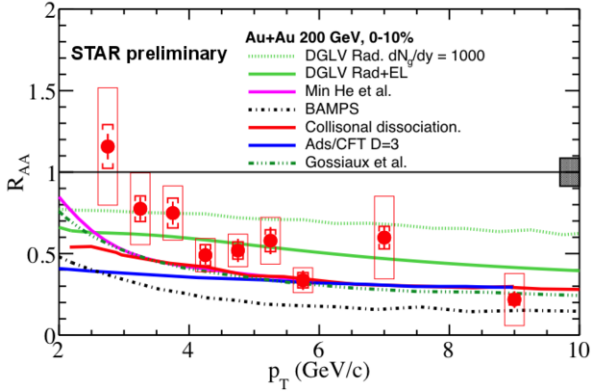

Figure 5: Non-photonic electron R_{AA} in central $\sqrt{s_{NN}}$=200 GeV Au+Au collisions compared to several models [24–28].

Figure 6: Non-photonic electron R_{AA} in $\sqrt{s_{NN}}$=62.4 GeV Au+Au collisions. The p+p reference used here is from pQCD calculations with k_T-factorization technique [29].

Figure 7: Non-photonic electron v_2 in $\sqrt{s_{NN}}$ =39, 62.4 and 200 GeV Au+Au collisions [10].

$b\bar{b}$ processes, which are accounted for using a simultaneous fit with templates of pre-set shapes from models, together with the signal.

3.1. Suppression and flow of the J/ψ

The J/ψ nuclear modification factor is shown in Fig. 8 for $\sqrt{s_{NN}}$ =39, 62.4 and 200 GeV Au+Au collisions as a function of N_{part}. Minimum bias U+U data at $\sqrt{s_{NN}}$ =193 GeV is also shown on the plot. Due to the lack of p+p data with sufficient statistics, Color Evaporation Model (CEM) predictions [16] are used as 39 and 62.4 GeV references. A significant suppression is observed at all energies in mid-peripheral to central collisions, and all four datasets are consistent with each other within uncertainties. Model predictions from Zhao and Rapp [31] are consistent with data. This model includes
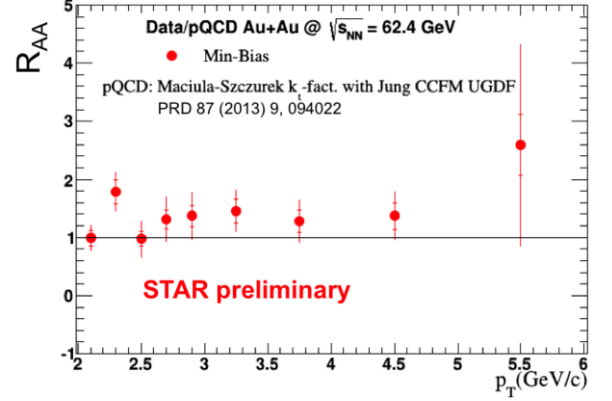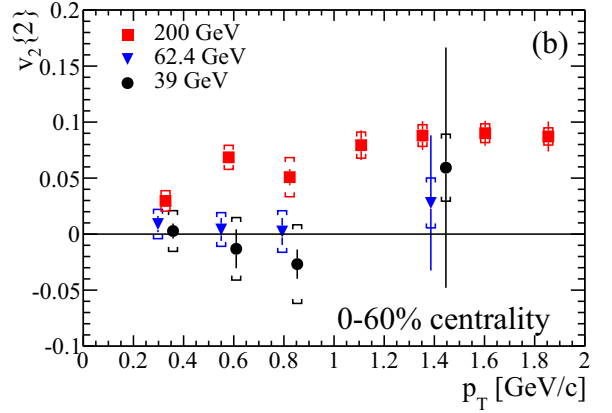
in-medium dissociation of the J/ψ as well as later regeneration from $c\bar{c}$ pairs. The weak dependence on collision energy predicted by the model and seen in the data suggests that different contributions that modify the J/ψ yield largely cancel each other in the observed R_{AA}.

The different contributions to the J/ψ suppression are, however, momentum-dependent. High-p_T J/ψ production is much less affected by CNM effects as well as regeneration in the later stages, and hot nuclear modification becomes the dominant factor [31]. Fig. 9 shows the R_{AA} for high-momentum (p_T>5 GeV) J/ψ mesons. In central collisions one still observes a significant suppression that is consistent with the minimum bias data, while in the case of peripheral collisions it is gone and R_{AA} is consistent with unity. It is to be noted that the current STAR J/ψ measurements are inclusive, where the contribution from B meson
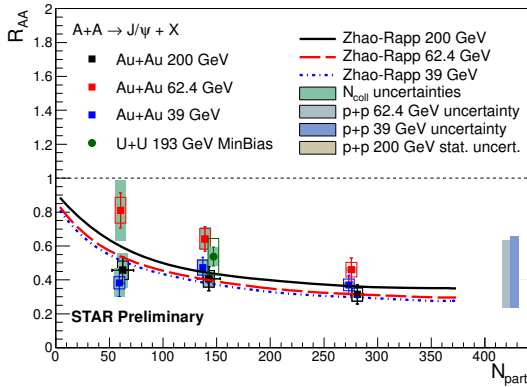
Figure 8: Low-momentum (p_T<5 GeV/c) J/ψ nuclear modification factor vs. the number of participants in $\sqrt{s_{NN}}$ =39, 62.4 and 200 GeV Au+Au and 194 GeV U+U collisions (black, red, blue squares and a green dot, respectively), compared to a model calculation [31].

feed-down can be as high as 15–25% above p_T=5 GeV. The model of Ref. [31] underpredicts the change in peripheral R_{AA} when going from p_T-integrated to high-momentum data. However, the model of Liu *et al.* [33], which includes the same main components but also considers melting of excited charmonium states feeding down to J/ψ, provides good description to the data.

Those J/ψ mesons that are created late in the reaction may be thermalized and thus they may take part in the collective motion that the bulk of hadrons exhibit. Fig. 10 shows the azimuthal anisotropy parameter v_2 of the J/ψ mesons in minimum bias data. Above p_T>2 GeV, STAR data shows complete consistency with the non-flow estimation, unlike v_2 of light mesons and the ϕ mesons [13]. This renders the scenario unlikely where J/ψ mesons mainly stem from late, thermalized coalescence of $c\bar{c}$ pairs [34], and supports early production of a significant fraction of the J/ψ mesons [35, 36].

3.2. Suppression of the Υ states

Nuclear modification factors of the Υ(1S+2S+3S) in $\sqrt{s_{NN}}$=200 GeV d+Au, Au+Au and new $\sqrt{s_{NN}}$=193 GeV U+U collisions are presented in Fig. 11 with respect to the number of participant nucleons. The trend observed in Au+Au is generally continued in the U+U data, with an R_{AA}=0.35±0.17(stat.)$^{+0.03}_{-0.13}$(syst.) measured for the 10% most central U+U collisions. The model of Strickland and Bazow [37] incorporates lattice QCD results on screening and broadening of bottomonium and the dynamical propagation of the Υ meson in the colored medium. Assuming an initial temperature between 428<T<443 MeV, the scenario with a potential based on heavy quark internal energy is consistent with
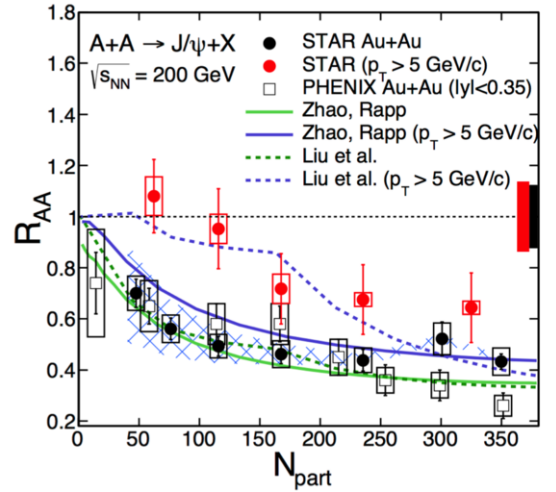

Figure 9: J/ψ nuclear modification factor in $\sqrt{s_{NN}}$ =200 GeV Au+Au collisions from STAR (black dots) [11] and PHENIX (open circles) [32], and STAR high-momentum-only (p_T >5 GeV/c) J/ψ R_{AA} (red dots) [12] vs. the number of participant nucleons, compared to model calculations [31, 33].

the observations, while the free energy based scenario is disfavoured. The strong binding scenario in model proposed by Emerick, Zhao, and Rapp [38], which includes possible CNM effects in addition, is also consistent with STAR results. It is to be noted, however, that STAR observed a suppression beyond model predictions of Υ in $\sqrt{s_{NN}}$ = 200 GeV d+Au collisions [14], which indicates that further investigation of CNM effects is necessary. This will be made possible by the upcoming year 2015 high-luminosity p+Au run.

4. Future prospects

In recent years, two new detectors have been installed that facilitate the ongoing heavy flavor program of STAR, the Muon Telescope Detector (MTD) and the Heavy Flavor Tracker (HFT). Both the MTD and the HFT were operational and taking data with dedicated trigger setups in the 2014 high-statistics Au+Au run.

The MTD [39] is a multi-gap resistive plate chamber that is located outside the STAR magnet, and covers 45% of the $|\eta|$<0.5 region. It is capable of detecting muons with ≈90% efficiency up to p_T =20 GeV/c along with good hadron rejection power. MTD allows for precision quarkonium R_{AA} and v_2 measurements. Fig. 12 shows the precision on R_{AA} versus N_{part} anticipated in the Υ (nS)→$\mu^+\mu^-$ channel for the three states separately.

The HFT [40] is a silicon microvertex detector system consisting of three subdetectors. Two layers of
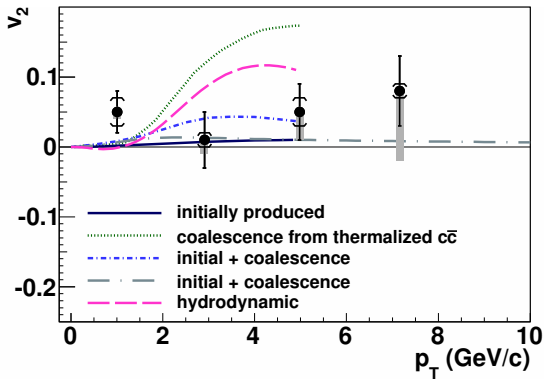
Figure 10: Azimuthal anisotropy v_2 of the J/ψ mesons in minimum bias data [13], compared to model calculations (lines). The shaded boxes represent the possible extent of the non-flow contribution.
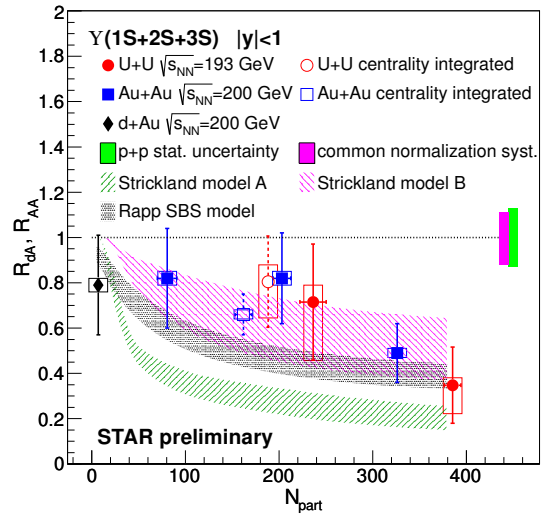

Figure 11: Υ nuclear modification factor in $\sqrt{s_{NN}}$ =200 GeV d+Au (rhombus) and Au+Au (squares) [14], as well as new preliminary $\sqrt{s_{NN}}$ =193 GeV U+U collisions (circles), compared to model calculations from Refs. [37, 38].

silicon pixel detectors (PXL) are located around the beampipe. The Intermediate Silicon Tracker (IST) is a single layer of silicon pad detectors. The outermost layer is the double-sided Silicon Strip Detector (SSD). The HFT makes it possible to reconstruct a secondary vertex with 20 μm precision. Note that the typical displacement of $D^0 \to K^-\pi^+$, $\Lambda_c^+ \to pK^-\pi^+$ and $B^\pm \to J/\psi + X$ secondary vertices are $c\tau \approx 120$, 60 and 500 μm, respectively. Thus, through the topological reconstruction of heavy flavor decays, HFT allows for precision measurements of open heavy flavor production and flow, as well as for the separation of prompt and non-prompt J/ψ contributions. As an example, Fig. 13 shows the projected uncertainties of the D^0 v_2 measurements in $\sqrt{s_{NN}}$=200 GeV Au+Au collisions.

5. Summary

A selection of recent heavy flavor measurements has been presented here. Total charm production cross sections from p+p D^0 and D^* measurements and Au+Au D^0 measurements at three different centralities are consistent with N_{bin} scaling, which supports the picture that charm is mainly produced in initial hard processes. The production of D^0 in top RHIC energy central heavy ion collisions at p_T>2 GeV/c shows a substantial suppression similar to light hadrons, suggesting a strong charm–medium interaction, while the hump-like structure at 1<p_T<2 GeV/c suggests charm–light quark coalescence. While $\sqrt{s_{NN}}$=200 GeV non-photonic electron measurements exhibit both a strong suppression and substantial anisotropy v_2, $\sqrt{s_{NN}}$=62.4 GeV R_{AA} shows no trace of suppression, and $\sqrt{s_{NN}}$=62.4 and 39 GeV v_2 measurements are consistent with no flow, sug-

gesting a radical change in heavy flavor production and dynamics between $\sqrt{s_{NN}}$=62.4 and 200 GeV energies.

The J/ψ R_{AA} also shows a strong suppression, but with a weak beam energy dependence. The U+U minimum bias data are consistent with the Au+Au measurements within errors. On the other hand, the measured v_2 for J/ψ is consistent with non-flow, thus rendering the thermalized $c\bar{c}$ coalescence scenario unlikely. The high-p_T J/ψ production, less influenced by regeneration and CNM effects, is also significantly suppressed in $\sqrt{s_{NN}}$=200 GeV central Au+Au collisions, which is a clear signal of the sQGP. This conclusion is further supported by the quantitatively similar suppression of Υ(1S), and that the Υ(2S) and Υ(3S) states are consistent with a complete suppression [14]. Cold nuclear matter effects, however, may play an important role in the case of Υ. The Υ(1S+2S+3S) R_{AA} versus N_{part} seems to follow a universal trend in d+Au, Au+Au and U+U, which is consistent with an sQGP initial temperature 428<T<443 MeV, according to a model which assumes an internal energy based potential [37].
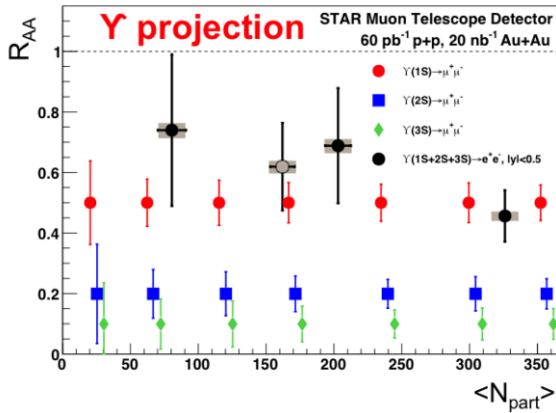
Figure 12: Anticipated statistical uncertainties on R_{AA} as a function of N_{part} measured in $\sqrt{s_{NN}}$=200 GeV Au+Au collisions the $\Upsilon \rightarrow \mu^+\mu^-$ channel for $\Upsilon(1S)$ (red), $\Upsilon(2S)$ (blue) and $\Upsilon(3S)$ (green) separately. The $\Upsilon(1S+2S+3S)$ measured with the BEMC in the electron channel (black) is plotted for comparison purposes.
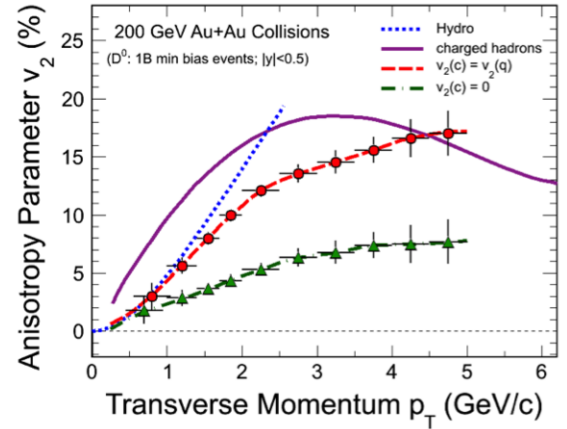

Figure 13: Anticipated D^0 v_2 statistical uncertainties versus p_T in $\sqrt{s_{NN}}$=200 GeV Au+Au collisions for the scenario when charm and light quarks flow similarly (red) and when charm has no flow (green).

References

[1] J. Adams *et al.* [STAR Collaboration], Nucl. Phys. A **757**, 102 (2005) [nucl-ex/0501009].

[2] A. Adare *et al.* [PHENIX Collaboration], Phys. Rev. Lett. **104**, 132301 (2010) [arXiv:0804.4168 [nucl-ex]].

[3] M. M. Aggarwal *et al.* [STAR Collaboration], arXiv:1007.2613 [nucl-ex].

[4] A. Mócsy and P. Petreczky, Phys. Rev. Lett. **99**, 211602 (2007) [arXiv:0706.2183 [hep-ph]].

[5] M. I. Gorenstein, A. P. Kostyuk, H. Stöcker and W. Greiner, Phys. Lett. B **509**, 277 (2001) [hep-ph/0010148].

[6] R. Rapp, D. Blaschke and P. Crochet, Prog. Part. Nucl. Phys. **65**, 209 (2010) [arXiv:0807.2470 [hep-ph]].

[7] K. H. Ackermann *et al.* [STAR Collaboration], Nucl. Instrum. Meth. A **499**, 624 (2003).

[8] L. Adamczyk *et al.* [STAR Collaboration], Phys. Rev. D **86**, 072013 (2012) [arXiv:1204.4244 [nucl-ex]].

[9] L. Adamczyk *et al.* [STAR Collaboration], accepted in PRL, arXiv:1404.6185 [nucl-ex].

[10] L. Adamczyk *et al.* [STAR Collaboration], arXiv:1405.6348 [hep-ex] (submitted to PLB).

[11] L. Adamczyk *et al.* [STAR Collaboration], Phys. Rev. C **90**, 024906 (2014) [arXiv:1310.3563 [nucl-ex]].

[12] L. Adamczyk *et al.* [STAR Collaboration], Phys. Lett. B **722**, 55 (2013) [arXiv:1208.2736 [nucl-ex]].

[13] L. Adamczyk *et al.* [STAR Collaboration], Phys. Rev. Lett. **111**, no. 5, 052301 (2013)

[14] L. Adamczyk *et al.* [STAR Collaboration], Phys. Lett. B **735**, 127 (2014) [arXiv:1312.3675 [nucl-ex]].ri

[15] D. Kikoła, G. Odyniec and R. Vogt, Phys. Rev. C **84**, 054907 (2011) [arXiv:1111.4693 [nucl-ex]].

[16] R. E. Nelson, R. Vogt and A. D. Frawley, Phys. Rev. C **87**, 014908 (2013) [arXiv:1210.4610 [hep-ph]].

[17] B. I. Abelev *et al.* [STAR Collaboration], Phys. Lett. B **655**, 104 (2007) [nucl-ex/0703040].

[18] G. Agakishiev *et al.* [STAR Collaboration], Phys. Rev. Lett. **108** (2012) 072302 [arXiv:1110.0579 [nucl-ex]].

[19] R. Sharma, I. Vitev and B. W. Zhang, Phys. Rev. C **80**, 054902 (2009) [arXiv:0904.0032 [hep-ph]].

[20] M. He, R. J. Fries and R. Rapp, Phys. Rev. C **86**, 014903 (2012) [arXiv:1106.6006 [nucl-th]].

[21] P. B. Gossiaux, J. Aichelin, T. Gousset and V. Guiho, J. Phys. G **37**, 094019 (2010) [arXiv:1001.4166 [hep-ph]].

[22] S. Cao, G. Y. Qin and S. A. Bass, Phys. Rev. C **88**, no. 4, 044907 (2013) [arXiv:1308.0617 [nucl-th]].

[23] W. M. Alberico, A. Beraudo, A. De Pace, A. Molinari, M. Monteno, M. Nardi and F. Prino, Eur. Phys. J. C **71**, 1666 (2011) [arXiv:1101.6008 [hep-ph]].

[24] M. Djordjevic, M. Gyulassy, R. Vogt and S. Wicks, Phys. Lett. B **632**, 81 (2006) [nucl-th/0507019].

[25] A. Buzzatti and M. Gyulassy, Nucl. Phys. A **910-911**, 490 (2013) [arXiv:1207.6020 [hep-ph]].

[26] H. van Hees, M. Mannarelli, V. Greco and R. Rapp, Phys. Rev. Lett. **100**, 192301 (2008) [arXiv:0709.2884 [hep-ph]].

[27] R. Sharma, I. Vitev and B. W. Zhang, Phys. Rev. C **80**, 054902 (2009) [arXiv:0904.0032 [hep-ph]].

[28] W. A. Horowitz, *Ph.D thesis* (2010) arXiv:1011.4316 [nucl-th].

[29] R. Maciula and A. Szczurek, Phys. Rev. D **87**, no. 7, 074039 (2013) [arXiv:1301.4469 [hep-ph]].

[30] M. Basile *et al.*, Nuovo Cim. A **65**, 421 (1981).

[31] X. Zhao and R. Rapp, Phys. Rev. C **82**, 064905 (2010) [arXiv:1008.5328 [hep-ph]].

[32] A. Adare *et al.* [PHENIX Collaboration], Phys. Rev. Lett. **98**, 232301 (2007) [nucl-ex/0611020].

[33] Y. p. Liu, Z. Qu, N. Xu and P. f. Zhuang, Phys. Lett. B **678**, 72 (2009) [arXiv:0901.2757 [nucl-th]].

[34] L. Ravagli and R. Rapp, Phys. Lett. B **655**, 126 (2007) [arXiv:0705.0021 [hep-ph]].

[35] X. Zhao and R. Rapp, arXiv:0806.1239 [nucl-th].

[36] Y. Liu, N. Xu and P. Zhuang, Nucl. Phys. A **834**, 317C (2010) [arXiv:0910.0959 [nucl-th]].

[37] M. Strickland and D. Bazow, Nucl. Phys. A **879**, 25 (2012) [arXiv:1112.2761 [nucl-th]].

[38] A. Emerick, X. Zhao and R. Rapp, Eur. Phys. J. A **48**, 72 (2012) [arXiv:1111.6537 [hep-ph]].

[39] L. Ruan *et al.*, J. Phys. G **36**, 095001 (2009) [arXiv:0904.3774 [nucl-ex]].

[40] Z. Xu *et al.*, LBNL-PUB-5509.